Infrared response of silicon oxynitrides investigated by high-resolution electron-energy-loss spectroscopy

M. D. Diatezua and P. A. Thiry
Institute for Study in Interface Sciences, Laboratoire Interdisciplinaire de Spectroscopie Electronique, Facultés Universitaires Notre-Dame de la Paix, 61 rue de Bruxelles, B-5000 Namur, Belgium

Ph. Lambin
Institute for Study in Interface Studies, Laboratoire de Physique du Solide, Facultés Universitaires Notre-Dame de la Paix, 61 rue de Bruxelles, B-5000 Namur, Belgium

R. Caudano
Institute for Study in Interface Sciences, Laboratoire Interdisciplinaire de Spectroscopie Electronique, Facultés Universitaires Notre-Dame de la Paix, 61 rue de Bruxelles, B-5000 Namur, Belgium
(Received 29 March 1993; revised manuscript received 2 June 1993)

Silicon oxynitride films of various compositions were grown *in situ* by RF-plasma sputtering. The high-resolution electron-energy-loss spectra were analyzed in the framework of the dielectric theory after addition of a characteristic background structure. The evolution of the energy-loss peaks as a function of [N]/([N]+[O]) concentration ratio clearly exhibits a one-mode behavior. This suggests that silicon oxynitride is characterized by a mixture of Si-O and Si-N bonds at the atomic level. An exponential frequency shift of the main peak is observed as a function of the concentration ratio. Infrared optical parameter values are provided for thermal and RF-plasma sputtered oxides, and for two compositions of RF-plasma $SiO_xN_y[y/(y+x)=0.37$ and $0.80]$ silicon oxynitrides.

I. INTRODUCTION

Silicon oxide and silicon nitride are widely used in integrated circuit technology, particularly as passivation and masking layers. Both materials have complementary properties which several important applications make use of. However, they present some mutual disadvantages such as a poor diffusion barrier for silicon oxide and a lower band gap for electrical insulation in the case of silicon nitride. Silicon oxynitride combines the beneficial properties of these two materials in one compound, and consequently triggers a great interest nowadays in many applications for the microelectronic technology.[1]

On the other hand, due to its ability to change its infrared optical behavior, silicon oxynitride has been used as the basic material for developing systems transparent in the near-infrared and visible regions.[2] It is indeed because of the possibility of varying its main infrared-absorption frequency as a function of its chemical composition,[3] that silicon oxynitride became famous in the search for infrared selective materials.[4,5] The optical properties of silicon oxynitride have been widely studied by infrared spectroscopies, and some linear correspondence could be established between composition and many optical parameters.[6–8]

The most used method for preparing silicon oxynitride films is by low-pressure chemical vapor deposition (LPCVD), which consists of depositing the film on a heated substrate (400–900 °C) under a controlled atmosphere of SiH_2Cl_2, NH_3 and N_2O.[9] The stoichiometry of the film is monitored by varying the $[NH_3]/[N_2O]$ ratio of the gas concentrations. Several other mixtures of gases are also used. The composition can be tuned from pure silicon oxide to pure silicon nitride. The main problem of LPCVD is the difficulty in avoiding hydrogen incorporation in the film,[10] which can be harmful in cases other than electronic use.

Radio-frequency (RF)-plasma sputtering is another popular technique for producing silicon oxynitride.[11] It consists of sputtering a silicon target[12] at the cathode by a controlled nitrogen-oxygen plasma and depositing it on a substrate (the anode). Here again the chemical composition of the films is modified by varying the gas concentration ratio of the plasma.[13] The main advantage of the RF-plasma sputtering is that the film can be deposited on all substrates even at ambient temperature. Some authors add a little argon in the plasma in order to enhance the deposition rate.

Si_2ON_2 is the only crystalline form of silicon oxynitride. It is available as a powder. By contrast, all solid silicon oxynitride films prepared by the aforementioned techniques are amorphous. From the chemical point of view, silicon oxynitride is currently considered as a solid alloy of silicon oxide and silicon nitride, i.e., a composite material.[8] Under this scheme, covalent bonds link together SiO_2 and Si_3N_4 molecules, and consequently the vibrational structure of the composite material should exhibit a "two-mode behavior" with distinct SiO_2 and Si_3N_4 features. The observed one-mode behavior[11] that is confirmed by the present work suggests, on the contrary, that silicon oxynitride is characterized by a mixture of Si-O and Si-N bonds at the atomic level. In order to

0163-1829/93/48(12)/8701(8)/$06.00 ©1993 The American Physical Society

model the infrared optical response of such an alloy, the Maxwell-Garnet or Bruggemann effective-medium theories give good results.[14]

The study presented here reports on infrared data of RF-plasma sputtered silicon oxide and oxynitride films from high-resolution electron-energy-loss spectroscopy (HREELS) measurements. Several films of different compositions were prepared and analyzed. The paper is organized as follows: After a brief description of the experimental process in Sec. II, we shall detail in Sec. III the computational techniques based on the dielectric theory, including a phenomenological background that will be applied for processing the data.

Then in Sec. IV A, we will discuss qualitatively the HREELS spectra recorded on different kinds of pure silicon oxides. Their vibrational fingerprint consists of three main loss peaks at 480, 830, and 1170 cm^{-1}. In keeping with infrared literature,[15] the first peak is attributed to a rocking mode of the SiO_2 bonds, the second to their bending vibration, and the third to their stretching mode. We show that the intensity ratio between the former and latter peaks reflects the degree of amorphousness of the oxide.

In Secs. IV B and IV C, the HREELS spectra of silicon oxynitrides will be analyzed more precisely for two selected composition ratio [N]/([N]+[O])= 0.37 and 0.80. The HREELS spectra are characterized by two main loss peaks: The reminiscence of the SiO_2 rocking mode, whose amplitude decreases with increasing [N]/[O] ratio, and a two-component peak at higher frequency, the most intense feature. The latter structure shifts toward lower energy when the concentration ratio [N]/[O] increases, in agreement with infrared spectroscopic data.[6] This peak results from two vibrational modes: Si-N and Si-O stretching modes at 860 and 1170 cm^{-1}, respectively. A qualitative survey of HREELS spectra recorded on silicon oxynitrides over a wide range of composition shows clearly a one-mode behavior.

In Sec. IV E, we apply the dielectric theory to retrieve infrared optical constants from HREELS spectra of thermal and RF-sputtered silicon oxides as well as of two RF-sputtered oxynitrides [[N]/([N]+[O])=0.37 and 0.80].

II. EXPERIMENTAL PROCESSES

A detailed description of the experimental processes of our techniques of preparation, chemical characterization, and HREELS experiment has been presented elsewhere.[4,16] The silicon oxynitride samples were prepared by RF-plasma sputtering. The composition of the films was varied by changing the nitrogen/oxygen flux ratio. The exact stoichiometry was determined by Auger electron spectroscopy (AES) whose intensity was calibrated by Rutherford backscattering spectroscopy (RBS). HREELS experiments were performed in a separate UHV chamber in specular geometry, with electrons impinging on the surface at 7 eV. A second defocalized electron gun (2 keV) was used for neutralization of the charging effects.[17]

III. COMPUTATIONAL TECHNIQUES

A. Theory of HREELS

A HREELS spectrum recorded on a clean dielectric crystal exhibits loss and gain peaks caused, respectively, by the excitation and annihilation of surface phonons (Fuchs-Kliewer modes) which are long-wavelength optical vibrations. An amorphous material such as RF-plasma sputtered silicon oxynitride does not present long-range order as does a single crystal. Nevertheless there remains a local order (at short range), so that the concept of the phonon keeps its meaning. In the absence of long-range order, however, a better concept to use would be that of "the propagation of molecular vibrations." Direct consequences of the breaking of the long-range symmetry in amorphous materials are the broadening of optically active lines and the existence of more infrared active vibrational modes than in the crystalline configuration.[15] The ordered arrangement can be used as a zeroth-order approximation for the theoretical treatment of the amorphous arrangement.

The starting point for treating the spectral response of a solid in a HREELS experiment is via its bulk dielectric function $\varepsilon(\omega)$. The frequency ω_s of the Fuchs-Kliewer modes at the solid surface is deduced from the equation

$$\varepsilon(\omega_s) = -1 \ . \tag{1}$$

The surface vibrations ω_s are thus confined in the forbidden frequency bands between ω_{TO} and ω_{LO} where the dielectric function $\varepsilon(\omega)$ is negative.

The HREELS spectrum is further derived from the expression of the classical probability $P_{cl}(\omega)$, whose expression writes[18]

$$P_{cl}(\omega) = \frac{e^2}{4\pi\varepsilon_0 \hbar v_\perp} \frac{2}{\pi^2} \int\int_D \frac{q v_\perp^3}{[(\mathbf{q}\cdot\mathbf{v}_\parallel - \omega)^2 + (q\cdot v_\perp)^2]^2} \times \mathrm{Im}[g(\mathbf{q},\omega)] d^2q \ , \tag{2}$$

where $\mathbf{v}_\parallel$ and $v_\perp$ are parallel and normal components of the electron velocity at the surface, D is a domain of wave vectors $\mathbf{q}$ determined by the analyzer acceptance angle, and $g(\mathbf{q},\omega)$ is the long-wavelength surface dielectric response:

$$g(\mathbf{q},\omega) = \frac{\varepsilon(\omega) - 1}{\varepsilon(\omega) + 1} \ . \tag{3}$$

Expression (3) is valid for a semi-infinite, homogeneous isotropic crystal having $\varepsilon(\omega)$ as dielectric function. For a material showing n absorption bands in the infrared range, the dielectric function is a sum of n Lorentzian terms:

$$\varepsilon(\omega) = \varepsilon(\infty) + \sum_{k=1}^{n} \frac{Q_k \omega_{TO,k}^2}{\omega_{TO,k}^2 - \omega^2 - i\Gamma_k \omega} \tag{4}$$

where $\omega_{TO,k}$ is the bulk transverse-optical-phonon frequency, Q_k is the oscillator strength, and Γ_k the damping constant.

B. Computing process

For the particular case of an isotropic, homogeneous material, Eq. (2) factorizes in

$$P_{\rm cl}(\omega)=\frac{e^2}{4\pi\varepsilon_0\hbar v_\perp}W_\theta\left[\frac{\hbar\omega}{2E_0\phi_a}\right]\text{Im}\left[\frac{\varepsilon(\omega)-1}{\varepsilon(\omega)+1}\right]\Big/\omega\ . \tag{5}$$

W_θ is independent of the material; it is a function of $x=\hbar\omega/2E_0\phi_a$, which decreases continuously from $1(x=0)$ to 0 (x approaching infinity). W_θ also depend on the incident angle θ and on the opening angle ϕ_a of the energy analyzer:

$$W_\theta(x)\cong\frac{1}{(1+\alpha x)^2}\frac{1+\beta x+c_1x^2}{1+\beta x+c_2x}\ , \tag{6}$$

where

$$\alpha=\left[\frac{2}{\pi}\right]^2E(\theta)\ , \tag{7}$$

$$c_1=\frac{2}{\pi}\alpha^2\sin\theta\ , \tag{8}$$

$$c_2=\frac{3\alpha^2}{1-c_1}\ . \tag{9}$$

$E(\theta)$ is a complete elliptic integral of the second kind, and the β factor is adjusted numerically so as to best reproduce the exact values of W_θ in the energy-loss range of interest. All this is calculated inside the EELS program.[18] The second step of the computer processing is related to the multiple energy losses and gains. It is performed by the BOSON computer code.[18]

C. The background calculation

For the samples we are dealing with, there as some difficulties in fitting HREELS data because of the presence of a broad background distribution. Presently, no explanation can account for such a background. This background is empirically simulated in the computer program by assuming that a fraction A_b of the impinging electrons are "thermalized" into a broad energy distribution. The theoretical EELS spectrum is then convoluted with the following response function:

$$R'(\omega)=A_bb(\omega)+(1-A_b)R(\omega)\ , \tag{10}$$

where $R(\omega)$ is a standard instrumental response estimated by the sum of Lorentzian and Gaussian functions fitted to the elastic peak, with the weight $1-A_b$. In Eq. (10), $b(\omega)$ is some broad distribution aimed at reproducing the observed electron background.

IV. RESULTS AND DISCUSSION

The best HREELS spectra reported to date (resolution close to 8 cm^{-1}) (Ref. 19) have been obtained on single-crystalline samples. The resolution degrades rapidly (50–70 cm^{-1}) for polycrystalline samples. For an amorphous dielectric, the situation is even worse, so that the energy resolution achieved here is never better than 90 cm^{-1}.

A. HREELS on RF sputtered and thermal silicon oxides

Figures 1(a) and 1(b) display HREELS spectra recorded on RF-plasma sputtered silicon oxide [Fig. (1a)] and

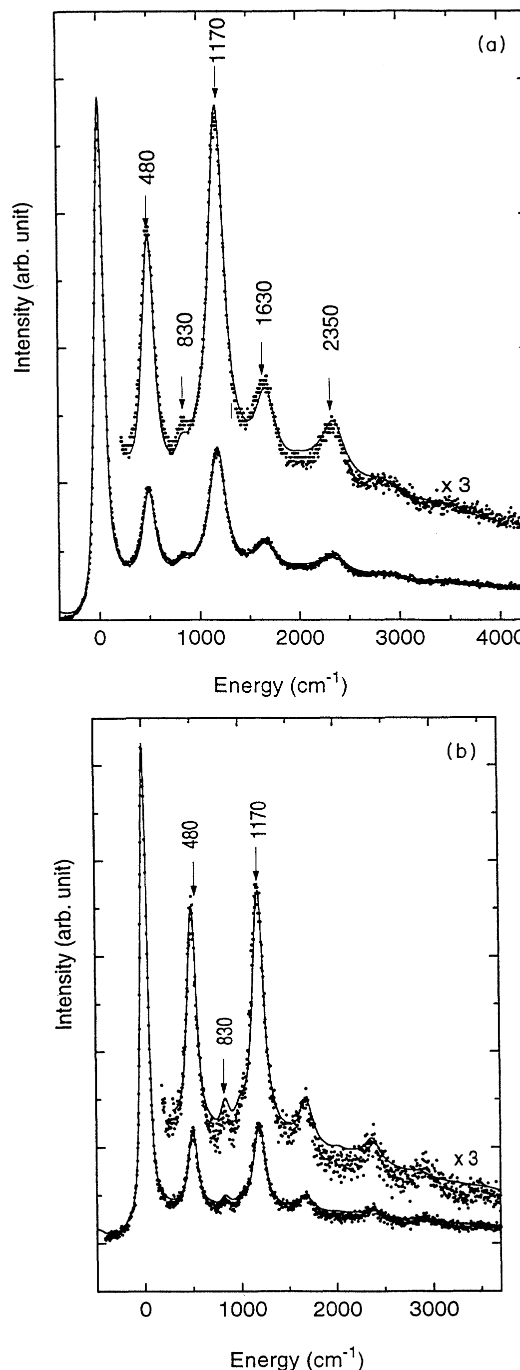

FIG. 1. HREELS spectra of a RF-plasma sputtered silicon oxide (a) and of a thermal silicon oxide (b). The solid lines represent the corresponding BOSON-fitted spectra.

thermal oxide [Fig. (1b)], respectively. Both spectra show three first-order loss peaks at 480, 830, and 1170 cm^{-1}; two second-order loss peaks at 1630 and 2350 cm^{-1} result from the combination of the two more intense first-order excitations.

In agreement with infrared spectroscopy results,[15] the first three peaks are attributed, respectively, to the rocking, bending, and stretching vibrations of the SiO_2 bond. The intensity ratio of the stretching and rocking modes is close to 1 for the thermal silicon oxide [Fig. 1(b)] and larger than 1 for the RF-plasma-sputtered oxide [Fig. 1(a)]. For crystalline silicon oxide (quartz), the corresponding rocking mode largely dominates the stretching one[20] (Fig. 2). We believe that the intensity ratio between rocking and stretching vibrations expresses the degree of amorphousness of the material. Indeed, in the more amorphous structure of RF-plasma sputtered silicon oxide, the rotations of the bonds, which are out-of plane displacements, are more easily quenched than the bending and stretching vibrations which are confined in the plane of the SiO_2 molecule.

B. Quantitative HREELS of RF-plasma sputtered silicon oxynitrides

Only two oxynitride compositions will be considered in this section: [N]/([N]+[O]) equals to 0.37 [Fig. 3(a)] and 0.80 [Fig. 3(b)]. In Figs. 3(a) and 3(b), the solid lines that are superimposed to the experimental points are the results of theoretical calculations using the above-described procedure aimed at determining infrared optical constants. The discussion on the theoretical treatment will be postponed to Sec. V, and we will deal here with a direct analysis of the experimental data, i.e., attribution of observed or eventually fitted peaks. Two main peaks appear in both spectra: one at 480 cm^{-1}, and another close to 1190 cm^{-1} for [N]/([N]+[O]) equal to 0.37, or around 1070 cm^{-1} for [N]/([N]+[O]) equal to 0.80. The peak at 480 cm^{-1} is the Si-O rocking vibration, the same as the one seen in the HREELS spectra of Fig. 1 albeit

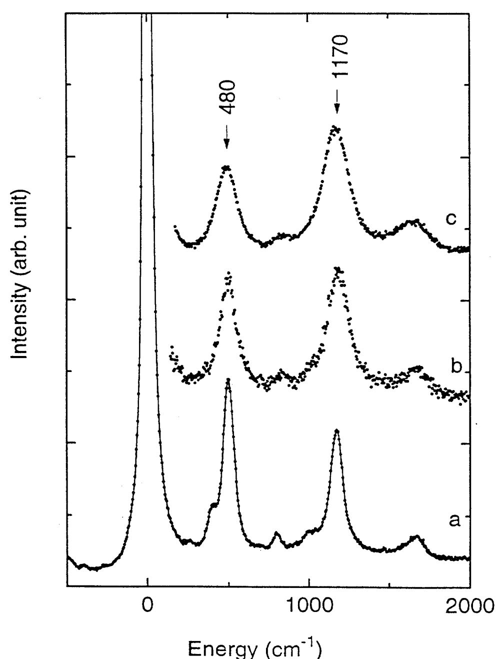

FIG. 2. HREELS spectra of quartz (a), thermal oxide (b), and RF-plasma-sputtered oxide (c).

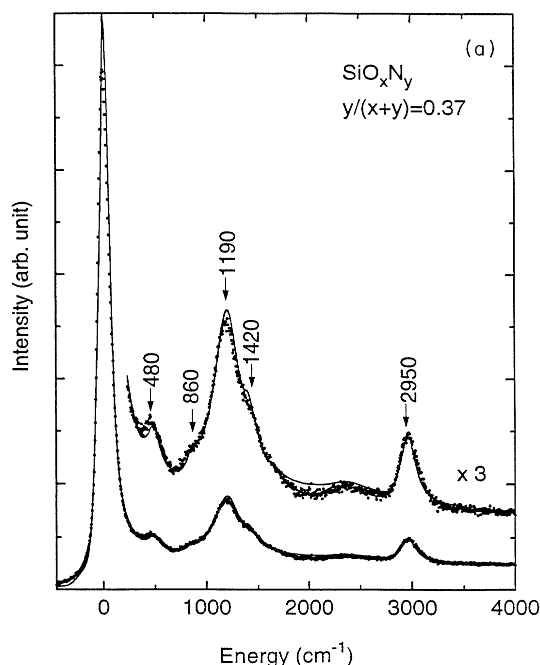

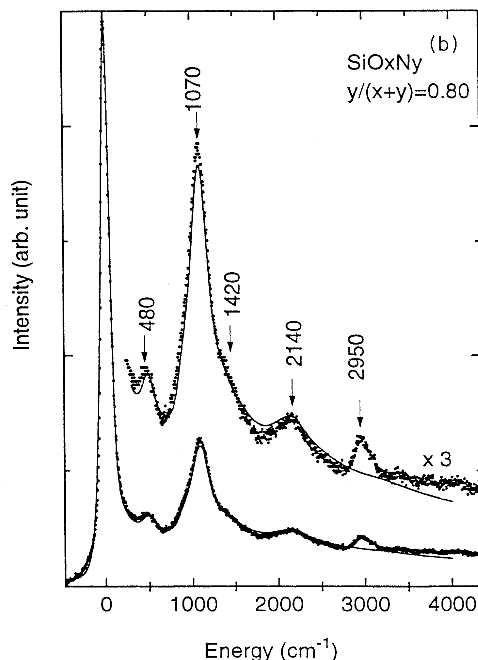

FIG. 3. HREELS spectra of a RF-plasma sputtered silicon oxynitride for [N]/([N]+[O])=0.37 (a) and 0.80 (b). The solid lines represent the corresponding BOSON-fitted spectra.

with less intensity because there is less oxygen in the oxynitride than in silicon oxide. On the other hand, Si-O and Si-N stretching vibrations contribute to the second main peak, that we now interpret separately for the two compositions:

1. *[N]/([N]+[O])=0.37 [Fig. 3(a)]*

The feature peak centered at 1190 cm^{-1} is a multiple-component structure. After a deconvolution process,[21] four components emerge: Three small ones at 910, 1420, and 1600 cm^{-1}, and a larger one at 1190 cm^{-1} [Fig. 4(a)] which dominates the structure. We believe that this component is a stretchinglike vibration characteristic of the 0.37 oxynitride [N]/([N]+[O]) ratio. This observation is in accordance with the expected one-mode behavior predicted by the consideration of the atomic mass ratio in silicon oxynitride as a consequence of the Chang-Mitra criterion.[22] Under this respect the stretching vibration in silicon oxynitride cannot be considered as a superposition of both Si-N and Si-O stretching modes. The small component around 910 cm^{-1} which causes the left asymmetry of the peak at 1190 cm^{-1} [Fig. 4(a)] is attributed to a mixing of Si-O and Si-N bending vibrations. The minority peak at 1420 cm^{-1}, also seen as a shoulder on Fig. 3(a), is attributed to a CH bending vibration of an important but unavoidable hydrocarbon contamination whose corresponding stretching vibration is at 2950 cm^{-1}. Indeed, the handbook of monomers and polymers[23] attributes the peak at 2950 cm^{-1} present in the spectra of Figs. 3(a) and 3(b) together with the 1420-cm^{-1} component [Figs. 4(a) and 4(b)] to the strong symmetric deformations of CH_3. The supplementary mode at 1600 cm^{-1} should be the first combination of the more intense first-order peaks, such as the peak at 1630 cm^{-1} from Figs. 1(a) and 1(b).

2. *[N]/([N]+[O])=0.80 [Fig. 3(b)]*

Two visible shoulders surround the main peak at 1070 cm^{-1} in this spectrum: at 890 and 1420 cm^{-1}. The deconvoluted spectrum[20] [Fig. 4(b)] indicates that the shoulder at 890 cm^{-1}, corresponds to the 910-cm^{-1} component of the previous spectrum [Fig. 4(a)]. All explanations given in the preceding paragraph also apply here, except that the CH vibration peak at 1420 cm^{-1} and the mode at 1600 cm^{-1} [Fig. 4(b)], here reproduced at 1650 cm^{-1}, are smaller than in the similar previous spectrum. The mode at 2140 cm^{-1} is the second-order peak corresponding to the Si-O stretching vibration

C. Qualitative HREELS of silicon oxynitride for different compositions

A stack of five spectra measured on five films of different compositions is presented in Fig. 5: [N]/([N]+[O]) equals to 0.0 (a), 0.1 (b), 0.14 (c), 0.53 (d), 0.8 (e), and 0.9 (f). As the ratio [N]/([N]+[O]) increases, the main loss peak shifts to lower energy. At the same time, the second peak regularly loses intensity. This proves the decrease of oxygen concentration and the corresponding increase of nitrogen. Within the limits of uncertainty of these results, an exponential dependence of the main absorption peak energy of the silicon oxynitride versus the ratio [N]/([N]+[O]) can be extracted. It is shown in Fig. 6.

D. Angular HREELS of silicon oxynitride

In a HREELS experiment, the electrons interact inelastically with the surface by three main channels:[17]

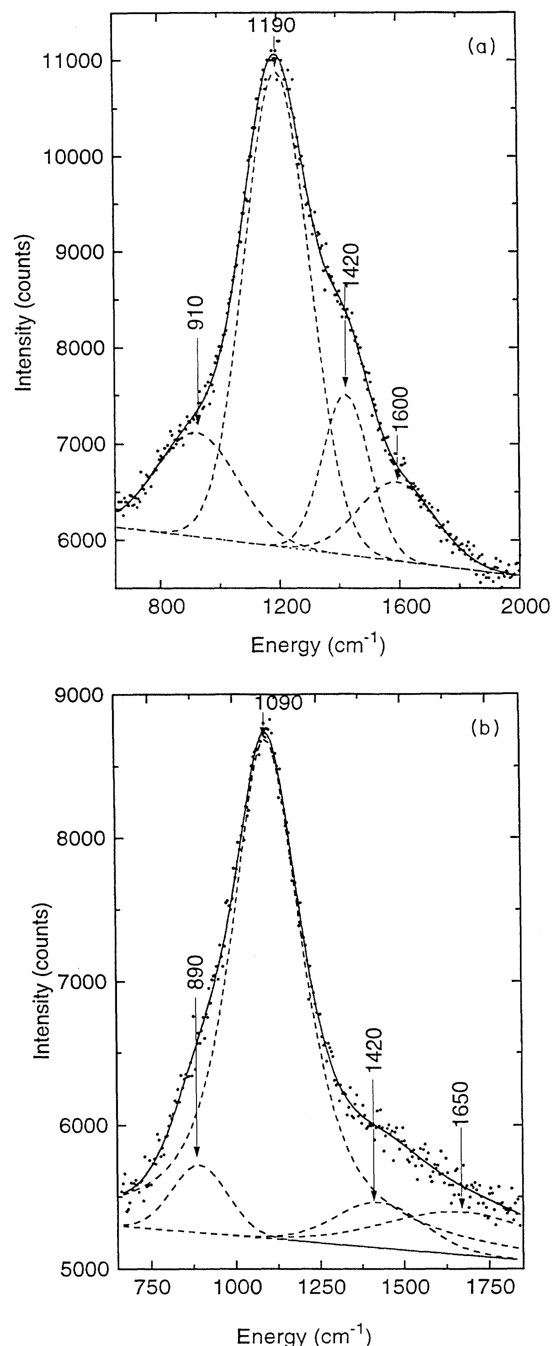

FIG. 4. Deconvoluted spectrum for [N]/([N]+[O])=0.37 (a) and 0.80 (b) from 600 to 2000 cm^{-1}.

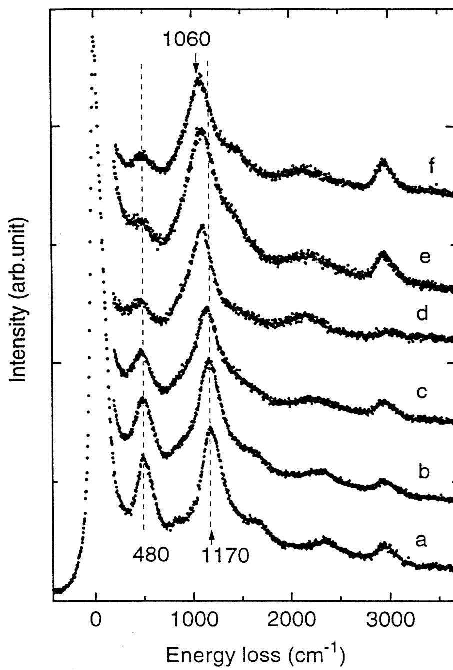

FIG. 5. Stacked HREELS spectra of RF-plasma sputtered silicon oxynitride for different values of [N]/([N]+[O]): (a) 0.0; (b) 0.10; (c) 0.14; (d) 0.53; (e) 0.80 and (f) 0.90.

By dipole scattering, i.e., by interaction of the electric field accompanying the electron with the dipole field of the elementary excitations of the target; by impact scattering i.e., the impinging electron being scattered by the atomic potentials; and by resonance scattering.

For a crystalline sample, the dipole-scattered electrons are concentrated in a sharp lobe surrounding the specular direction.[24] In the impact processes such a sharp lobe no longer exists. Consequently, by varying the analysis angle it is possible to distinguish between the losses arising from one or another scattering channel.

The specular lobe aperture is wide in the case of a polycrystalline sample. This lobe, i.e., the preferential analysis direction, no longer exists for amorphous samples. As shown from Fig. 7, that presents a sequence of four HREELS spectra of silicon oxynitride taken at different analysis angles, no differences are evident between these spectra. This fact confirms the amorphous character of the RF-sputtered silicon oxynitride.

E. Optical constants of silicon oxides and oxynitrides

As shown above, the presence of a noncharacterized background present in the insulator HREELS spectra does not allow the use of regular methods of exploiting HREELS data. The necessary background structure is introduced in the computing program by a fitting procedure.

The first step in deducing the optical parameters is the

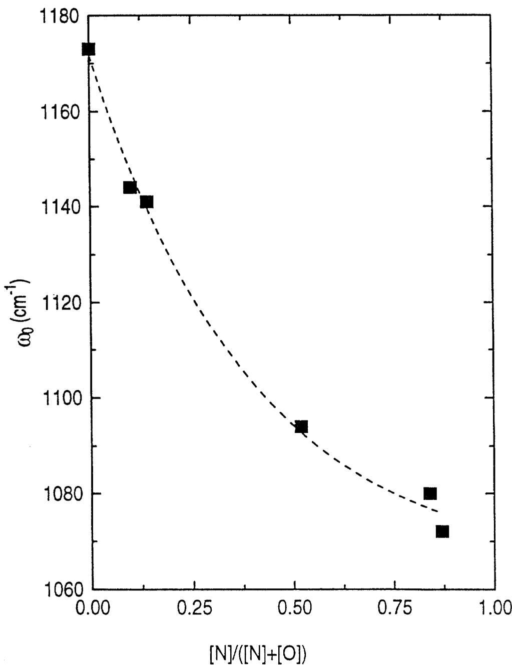

FIG. 6. Evolution of the more intense peak energy vs [N]/([N]+[O]). The exponential curve is fitted to the points: $E_0 = Ae^{-bx}$, $A = 107.6$, and $b = 2.53$; the correlation coefficient is 0.995.

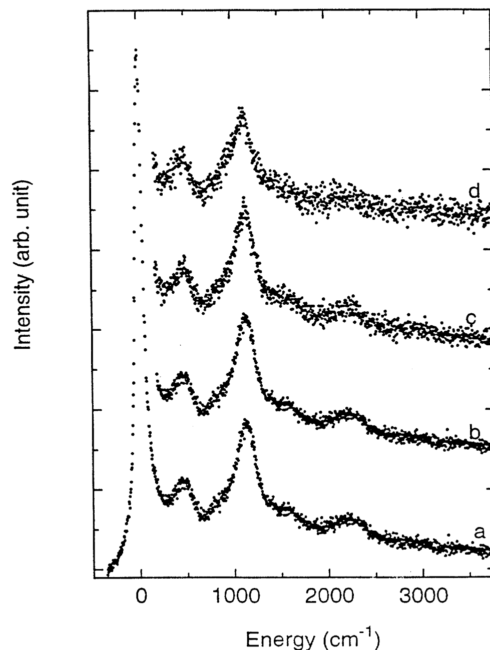

FIG. 7. Stacked HREELS spectra of RF-plasma sputtered silicon oxynitride for four analysis angles: (a) specular direction (45°); (b) 60°; (c) 70°; and (d) 75°.

modeling of the dielectric function. We know that the best silicon oxynitride model dielectric function can be obtained with a random mixture of SiO_jN_{4-j} ($j=0,\ldots,4$) tetrahedra representation, including the second-neighbor interaction in the network of the Bruggemann effective-medium theory. However, instead of calculating the dielectric function from the Bruggemann theory, we shall use a simple three-oscillator model [Eq. (4) with $n=3$]. The starting computing parameters were selected values from crystalline silicon dioxide.[25] The resulting values (Table I) are those which provided the best fit to the experimental spectra of Figs. 1 and 3. The solid curves superimposed on the experimental points on Figs. 1(a) and 1(b) and 3(a) and 3(b) are the result of the theoretical calculations using a three-oscillator model for silicon oxide and oxynitride. However, in the case of silicon oxynitride having a concentration ratio of 0.37 [Fig. 3(a)] a supplementary CH oscillator was introduced in order to account for the important hydrocarbon contamination. The parameters of this fourth oscillator have of course been omitted in Table I. Because of the lower level of contamination observed in the 0.80 oxynitride, this feature was not added on theoretical simulation of Fig. 3(b).

The modifications of the silicon oxide[26] resonance frequencies ω_{TO} are small compared to the instrumental resolution, and consequently they do not reveal any significant difference, except for the third oscillator whose frequency shifts from 1020 (thermal oxide) to 920 cm^{-1} (RF-plasma oxide). The large differences between oscillator strengths could result from our background treatment. Note that the damping constant of the oscillators are larger for RF-plasma sputtered oxides. This is a consequence of their higher degree of amorphousness, already emphasized in Sec. IV A. Indeed, the disorder opens new deexcitation channels for the vibrations and hence reduces their lifetimes. Nevertheless, the importance of the damping is probably also exaggerated by the background treatment. The starting value of $\varepsilon(\infty)$ has been taken from the literature.[25] It is not very sensitive to the amorphousness of the oxide,and large deviations were observed only for silicon oxynitrides with very low oxygen concentration.

For the silicon oxynitride with $[N]/([N]+[O])=0.37$, the main result is the ratio between the oscillator strengths of the modes at 990 and 820 cm^{-1}. This ratio is inverted for $[N]/([N]+[O])$ equal to 0.8. This highlights the fact that the three-oscillator model in silicon oxynitride attributes the oscillator at 820 or 840 cm^{-1} to Si-N vibrations, and the one at 990 or 950 cm^{-1} to Si-O bonds. On the other hand, the high-frequency limit of the dielectric function increases from 2.42 (for $[N]/([N]+[O])=0.37$) to 2.85 [for $[N]/([N]+[O]) = 0.80$], reflecting a monotonous variation from the value of silicon oxide to the higher value of silicon nitride.

In a previous paper[16] we have described HREELS measurements performed during sputtering of a $SiO_{1.3}N_{0.6}$ oxynitride film deposited on an Al metallized Si(100) substrate. In that case, the appearance and the development, after substantial sputtering time, of a peak at 880 cm^{-1} was attributed to the Si-N Fuchs-Kliewer mode of a pure nitride layer located at the interface. Hence, a two-mode behavior was tentatively inferred. RBS measurements performed on the same layer deposited on an Al-metallized graphite substrate indeed indicated the segregation of nitrogen at the interface. However, the results obtained in the present paper on better defined systems, and without sputtering, call for a reinterpretation of the previous experiments, as the one-mode behavior is now unambiguously established. HREELS experiments carried out in our laboratory on Al oxides and nitrides reveal spectral contributions around 800 cm^{-1} for the oxides, and 860 cm^{-1} for the nitrides, so that it is very likely that the broad structure observed at 880 cm^{-1} was partly due to sputter-induced nitridation and oxidation of Al at the interface. As no chemical analysis was performed after sputtering, the exact vibrational contribution of silicon oxynitride could not be clearly identified, and the related conclusion drawn at that time about the mode behavior is not reliable.

TABLE I. Infrared optical parameters of silicon oxides and oxynitrides determined from HREELS measurements.

Sample	ω_{TO} (cm^{-1})	Γ (cm^{-1})	Q	$\varepsilon(\infty)$
Thermal SiO_x	440	3.00	1.40	
	815	8.15	0.19	2.42
	1020	66.00	1.05	
RF-plasma SiO_x	410	47.25	2.70	
	785	11.0	0.34	2.42
	920	105.0	1.70	
RF-plasma SiO_xN_y	460	11.5	0.20	2.42
	820	4.0	0.20	
$\frac{y}{x+y}=0.37$	990	198	1.85	
RF-plasma SiO_xN_y	460	87.4	0.40	
	840	100.0	1.60	2.85
$\frac{y}{x+y}=0.80$	950	133.0	0.50	

V. CONCLUSION

The dielectric function of silicon oxide and silicon oxynitride has been determined from HREELS measurements. The vibrational fingerprint of RF-plasma sputtered materials confirms the picture of silicon oxynitride as a mixture of Si-N and Si-O bonds at the atomic level, agreeing with the Bruggemann theory in that. A quantitative interpretation of the EELS spectra is not possible in the framework of the dielectric theory, without taking account of a phenomenological "background" contribution. The parameters of the dielectric function are given for thermal and RF-plasma sputtered silicon oxide and for two RF-plasma sputtered silicon oxynitrides of different composition.

ACKNOWLEDGMENTS

Ph.L. thanks the Belgian NFSR for financial support. This work presents research results of the Belgian programme on Interuniversity Research Project (PAI) initiated by the Belgian State, Prime Minister's office, Science Policy Programming. We acknowledge the financial support of the Belgian National Fund for Scientific Research.

[1] J. Robertson and M. J. Powell, Appl. Phys. Lett. **44**, 415 (1984).

[2] D. E. Aspnes and J. B. Theeten, J. Appl. Phys. **50**, 4928 (1979).

[3] T. S. Eriksson and C. G. Granqvist, J. Appl. Phys. **60**, 2081 (1986).

[4] M. D. Diatezua, A. Dereux, A. Ronda, Ph. Lambin, J.-P. Vigneron, and R. Caudano, Proc. SPIE **1149**, 80 (1989).

[5] T. S. Eriksson, E. M. Lushiku, and C. G. Granqvist, Sol. Energy Mater. **11**, 149 (1984).

[6] S. C. Audisio and H. Leidheiser, J. Electrochem. Soc. **119**, 408 (1972).

[7] A. K. Gaind, G. K. Ackermann, V. J. Lucarini, and R. L. Bratter, J. Electrochem. Soc. **124**, 599 (1977).

[8] T. Baak, Appl. Opt. **21**, 1068 (1982).

[9] F. H. P. M. Habraken, Appl. Surf. Sci. **30**, 186 (1987).

[10] J. B. Oude Elferink, U. A. Van Der Heide, W. M. Arnold Bik, F. H. P. M. Habraken, and W. F. Van Der Weg, Appl. Surf. Sci. **30**, 197 (1987).

[11] M. S. Hedge, R. Carracciolo, K. S. Hatton, and J. B. Watchman, Jr., Appl. Surf. Sci. **37**, 16 (1989).

[12] B. Chapman, *Glow Discharge Process* (Wiley, New York, 1980).

[13] A. Ronda, M. D. Diatezua, A. Dereux, Ph. Lambin, J.-P. Vigneron, and R. Caudano, Le Vide-Les Couches Minces **245**, 96 (1989).

[14] G. A. Niklasson and C.G. Granqvist, J. Appl. Phys. **55**, 3382 (1984).

[15] Y. Cross, D. Jousse, J. Liu, and J. C. Rostaing, J. Non-Cryst. Solids **90**, 287 (1987).

[16] M. D. Diatezua, P. A. Thiry, G. Terwagne, and R. Caudano, Surf. Sci. **269**, 1054 (1992).

[17] J.-J. Pireaux, P. A. Thiry, R. Sporken, and R. Caudano, Surf. Interf. Anal. **15**, 189 (1990).

[18] Ph. Lambin, J.-P. Vigneron, and A. A. Lucas, Comput. Phys. Commun. **60**, 351 (1990).

[19] H. Ibach, *Electron Energy Loss Spectrometers* (Springer-Verlag, Berlin, 1991).

[20] P. A. Thiry, M. Liehr, J.-J. Pireaux, R. Caudano, J.-P. Vigneron, and A. A. Lucas, J. Vac. Sci. Technol. B **3**, 1118 (1985).

[21] SpectraCalc Program, Arithmetic A2.22, Galactic Industries Corp., copyright 1990.

[22] L. F. Chang and S. S. Mitra, Phys. Rev. **172**, 924 (1968).

[23] *The Infrared Spectra Atlas of Monomers and Polymers* (Sadtler Research Laboratories, Philadelphia, 1980).

[24] P. A. Thiry, M. Liehr, J.-J. Pireaux, and R. Caudano, Physica Scr. **35**, 368 (1987).

[25] Ph. Gaskell and D. W. Johnson, J. Cryst. Solids **20**, 153 (1976).